Macromolecular Materials and Engineering

Macromolecular Materials and Engineering Open Access

www.mame-journal.de

RESEARCH ARTICLE OPEN ACCESS

Impact of Formulation Ingredient Compatibility on Encapsulation of Hydrophobic Substances in Polymeric Nanocarriers Prepared by Nanoprecipitation

Mark Sabura[1,2] | Agnes-Valencia Weiss[1,2] | Svenja Pohl[3] | Guido Kickelbick[3] | Marc Schneider[1,2]

[1]Department of Pharmacy, Biopharmaceutics and Pharmaceutical Technology, Saarland University, Saarbrücken, Germany | [2]PharmaScienceHub (PSH), Saarbrücken, Germany | [3]Inorganic Solid-State Chemistry, Saarland University, Saarbrücken, Germany

Correspondence: Marc Schneider (marc.schneider@uni-saarland.de)

Received: 3 July 2025 | **Revised:** 7 October 2025 | **Accepted:** 8 October 2025

Keywords: atomic force microscopy | differential scanning calorimetry | drug loading | nanoparticles | solubility parameters

ABSTRACT

As a versatile platform technology, polymer nanoparticles enable the effective delivery of hydrophobic drug substances. To achieve therapeutic efficacy, adequate drug loading is required, which requires a quantitative understanding of formulation component affinities. In this study, we investigate how the choice of organic solvent affects drug loading in poly(lactic-*co*-glycolic) acid (PLGA) nanoparticles prepared by nanoprecipitation. For the encapsulation of various 1,4-naphthoquinone derivatives used as model substances, we observe a correlation between drug loading and the Hansen solubility parameter distance (R_a) between the drug and the organic solvents. To elucidate the interactions at the nanoscale level thin polymer films are analyzed using atomic force microscopy (AFM), quantifying surface pore formation as an indicator of interaction. Additionally, scanning electron microscopy (SEM) and differential scanning calorimetry (DSC) were utilized to investigate drug–polymer miscibility. A concentration-dependent phase separation in drug-polymer matrices was observed, which correlates with the drug loading in the nanoparticles. This work emphasizes the need to move beyond trial-and-error approaches by the incorporation of predictive parameters like Hansen solubility parameter-derived affinities and solid-state solubility metrics into formulation strategies.

1 | Introduction

Polymeric nanoparticles represent a promising drug delivery platform technology which overcomes the drawbacks of conventional formulations and enables the delivery of previously non-deliverable molecules [1–3]. The demand for novel drug delivery systems is growing, as a significant proportion of molecules in the discovery pipeline are insoluble in water [4]. Nano-drug delivery systems can be divided in four categories according to the underlying loading mechanism: molecular-level loading, surface loading, matrix loading, and cavity loading systems [5]. Formulating nanoparticles is often challenging, with adequate drug loading being a crucial factor for achieving therapeutic success [6]. In literature, two parameters have proven useful for describing the efficiency of a drug encapsulation process: drug loading (DL%) [7], i.e. the ratio of the mass of the encapsulated drug substance to the total mass of the particles, or encapsulation efficiency (EE%) [8], i.e. the ratio of the mass of the encapsulated drug substance to the mass of the drug substance used for the preparation. Both parameters have their strengths, EE% is well-suited for comparing the efficiency of encapsulation of different drug substances in a precisely defined system, as the influence of the molar mass is eliminated, and this gives a more accurate impression of the actual number of molecules interacting with the polymer [9]. As soon as the parameters of the nanoparticle preparation are changed, e.g.,

the organic solvent, the stabilizer, or the purification protocol, resulting in a change of the nanoparticle yield, DL% shows its strengths, since it reflects the proportion of drug within the final nanoparticle mass and allows comparisons across different formulation strategies or processing conditions. Both parameters are therefore complementary, and their suitability depends on the comparison being made. Nanoprecipitation is a well-described process for the preparation of polymeric nanoparticles, characterized by reproducibility and scalability, and is based on phase separation in a solvent-antisolvent system due to mixing. In addition, this can be influenced by changing physical conditions such as pH, salt concentration, or changes in solubility of the components [10]. In this study, we used the commonly used solvent displacement method [11, 12]. In this method, the polymer and the hydrophobic drug are dissolved in a water-miscible organic solvent and then added in a controlled manner to an aqueous phase containing a stabilizer. Precipitation is induced by reaching supersaturation, which leads to phase separation through nucleation and subsequent growth of polymer particles [10, 13]. Many studies have shown that the colloidal properties of nanoparticle formulations are influenced to a high degree by the physicochemical properties of the formulation components [14, 15]. In this context, it has also been shown that drug loading is significantly dependent on the polymer concentration [16], organic/aqueous phase ratio [17], drug concentration [18], and the affinity of the drug substance to the polymer matrix [19]. The logP value reflects the lipophilicity of a compound, describing its partitioning between octanol and water, and is a useful predictor of a drug's suitability for encapsulation in hydrophobic polymers, as molecules with higher logP values generally tend to exhibit higher loading in such systems [20, 21]. It is characterized by its simple determination, its relevance in biological questions, and its wide availability. As a one-dimensional parameter, the limitation of logP values lie in their own nature; more complex intermolecular interactions, solvent affinities, and precipitation kinetics can only be predicted to a limited extent. These limits can be partially exceeded by the Hansen solubility parameters (HSPs), which are widely used to predict compatibility between solvents, polymers, and other materials, aiding in processes like formulation and material design [22–24]. These solubility parameters (δ_D, δ_P, and δ_H) describe dispersive, polar, and hydrogen bonding interactions and provide three-dimensional measure of molecular compatibility and can be determined experimentally or calculated by group contribution methods [25, 26]. Due to the limited understanding of the precise mechanisms and relevant parameters that result in adequate drug loading, the formulation process is typically conducted through a trial-and-error approach, aimed at identifying the optimal conditions [27, 28]. To move beyond trial-and-error, a deep understanding of the underlying physicochemical properties is essential, enabling predictive power across polymers and drug classes, further enhanced by in silico approaches [29] and emerging AI-based tools [30]. The choice of the organic solvent for drug loading is often an overlooked yet critical influencing factor. Traditionally, drug loading is considered to be limited by the solubility of the drug substance in the organic solvent [9, 31]. In this study, we investigate whether drug loading correlates with the solvent's affinity for the drug, expressed as the Hansen solubility parameter distance (R_a). Different 1,4-naphthoquinone derivatives (plumbagin, menadione, and lawsone) were loaded into poly(lactic-*co*-glycolic) acid (PLGA) nanoparticles prepared by nanoprecipitation with varying organic solvents (Figure 1).

These compounds are suitable model substances due to their favorable solubility properties in the solvents used and their pharmaceutical relevance, as they exhibit anti-cancer, blood-thinning, and antimicrobial properties [32–36]. PLGA is a widely used pharmaceutical polymer valued for its biocompatibility, versatility, and favorable processing properties [37–39]. To elucidate solvent-dependent interactions at the nanoscale level, polymer films were prepared with the organic phase containing drug substances, and the morphology was analyzed using atomic force microscopy. Atomic force microscopy (AFM) is a powerful technique for analyzing interactions at the nanoscale level, offering unparalleled resolution and sensitivity [40]. This method is particularly suitable for analyzing sensitive samples, as it requires no treatment and preserves the samples during measurement. AFM is often used to analyze the morphology and nanostructure of nanomaterials containing drug substances, providing valuable insights about the interaction and physicochemical properties of the formulation components [41–44]. AFM facilitates the determination of various parameters that provide insights into the homogeneity and coherence of polymer films. Classically, surface roughness is the most prominent parameter to statistically represent topographical variations [45–47]. In this study, we focus on the spatial distribution of polymer film defects that manifest as pores due to drying effects of the drug-solvent-polymer system [48]. Our study shows that this pore formation is also dependent on the choice of solvent and the embedded drug substance. To quantify this effect, we determined the surface area exposed by the pores, allowing us to calculate the polymer film's coverage over a given area. This study further explores the potential relationship between the dewetting effects of polymer films on mica and the drug loading of the corresponding nanoparticles. In addition to solvent selection, drug–polymer miscibility is a key determinant of optimal drug loading [49]. Literature shows that scanning electron microscopy (SEM) effectively reveals the micro- and nanostructure of solid dispersions, providing insights into their compatibility and stability [50, 51]. To assess drug-polymer miscibility, polymer films with varying drug concentrations were prepared and analyzed using SEM. Special focus was placed on the concentration-dependent phase separation, offering relative insights into the solubility of drug substances within the polymer matrix. For the quantitative determination of solid-state solubility, PLGA-drug matrices were also analyzed using differential scanning calorimetry (DSC). DSC is a widely used thermal analysis technique that can determine the solid-state solubility of drugs in polymer matrices [9, 52, 53]. By analyzing thermal changes such as melting points, glass transitions, and possible recrystallization, DSC provides insights into the miscibility and molecular dispersion of the drug substance within a polymer matrix.

2 | Results and Discussion

2.1 | Influence of Drug-Solvent Affinity on DL%

Acetonitrile (ACN), acetone, dimethylformamide (DMF), and dimethyl sulfoxide (DMSO) are polar aprotic solvents and fre-

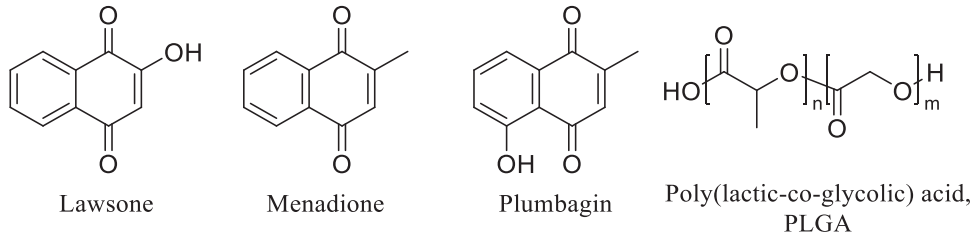

FIGURE 1 | Chemical structures of model drugs and PLGA.

TABLE 1 | Solubility parameters of lawsone, menadione, plumbagin and organic solvents.

	δ_D	δ_P	δ_H	R_a
Lawsone	21.3	14.5	12.1	
DMSO	18.4	16.4	10.2	6.39
DMF	17.4	13.7	11.3	7.88
Acetone	15.5	10.4	7	13.32
Acetonitrile	15.3	18	6.1	13.87
Menadione	20.0	12.3	6.2	
DMSO	18.4	16.4	10.2	6.56
DMF	17.4	13.7	11.3	7.42
Acetone	15.5	10.4	7	9.23
Acetonitrile	15.3	18	6.1	10.99
Plumbagin	19.7	13.1	11.1	
DMSO	18.4	16.4	10.2	4.30
DMF	17.4	13.7	11.3	4.64
Acetone	15.5	10.4	7	9.73
Acetonitrile	15.3	18	6.1	11.24

quently used in nanoprecipitation because they are fully miscible with water, provide excellent solubility for pharmaceutical polymers and active compounds, and can be readily removed by evaporation or centrifugation [54]. For effective nanocarrier-based therapy, maximizing drug loading is essential to minimize the required amount of nanoparticles to reduce potential carrier-associated toxicity [55]. In nanoparticle formulation, a high solubility of the drug in the organic phase is favorable, as it allows for a potentially increased drug load.

The HSPs of lawsone, menadione, and plumbagin were estimated using the Y-MB (Yamamoto Molecular Breaking) method implemented in the HSPiP software (Hansen Solubility Parameters in Practice, version 5.4.03, Hansen-Solubility.com, UK) while solvent solubility parameters were taken from the built-in database [56]. The R_a values were calculated to estimate the affinity between each drug substance and the used solvents (Table 1). Due to the chemical similarity of the drugs, the affinity order toward the solvents is consistent: R_a is lowest with DMSO, followed by DMF and acetone, and highest with ACN.

For each solvent, drug loading increased in the order: lawsone < menadione < plumbagin (Figure 2a). These significant differences are most likely due to the different affinities to PLGA, which will be discussed further below. Drug loading of the model substances correlated approximately linearly with the R_a values between the drug and the solvent (Figure 2b) with menadione and plumbagin showing significant increases (Figure S1). As previously mentioned, sufficient solubility of the drug substance in the organic solvent is essential for achieving high drug loading. However, once the general solubility threshold for the process is met—i.e., the amount of drug substance to be encapsulated is fully soluble in the organic phase—the specific affinity between the drug and the solvent becomes a determining factor. In such cases, a lower affinity, indicated by a higher R_a, was found to result in increased drug loading. Although the underlying molecular mechanisms remain unclear, it can be hypothesized that a reduced affinity of the drug for the organic solvent may lower its solubility in the solvent–non-solvent mixture, promoting its encapsulation in the polymer phase. It is important to note that lawsone, despite exhibiting the highest R_a toward the tested solvents consistently showed the lowest DL%. This discrepancy can be explained by its poor miscibility with PLGA, as evidenced by the SEM analysis (Section 2.4). Thus, drug loading is not only determined by drug-solvent affinity but by the interplay between drug-solvent and drug-polymer interactions. Across all tested 1,4-naphthoquinone derivatives, ACN consistently resulted in the highest DL%. This observation suggests that ACN may represent a favorable solvent choice under conditions where the drug–solvent affinity is sufficiently low to promote partitioning into the polymer phase. However, based on our data, it cannot be concluded that ACN will generally produce the highest DL% for all compound classes. Rather, the effect appears to be linked to the specific balance between solvent–drug and solvent–polymer interactions. The relatively moderate polarity and aromatic scaffold of the naphthoquinones may explain why ACN optimally reduces drug-solvent affinity while still maintaining sufficient solubility. For structurally distinct drug classes with different hydrogen bonding or lipophilicity profiles, different solvents might lead to a higher DL%. Our data reveals a consistent trend within this scaffold, to assess the potential generalizability of this concept, structurally diverse drug classes need to be systematically investigated.

2.2 | Effect of Solvent-Water Compatibility on Colloidal Properties

The nanoprecipitation process is driven by solvent diffusion and interfacial turbulence, which leads to rapid supersaturation and subsequent precipitation of nano-sized particles [57]. The choice of the organic solvent significantly influences colloidal properties of polymeric nanoformulations [14, 15]. It has been shown that the

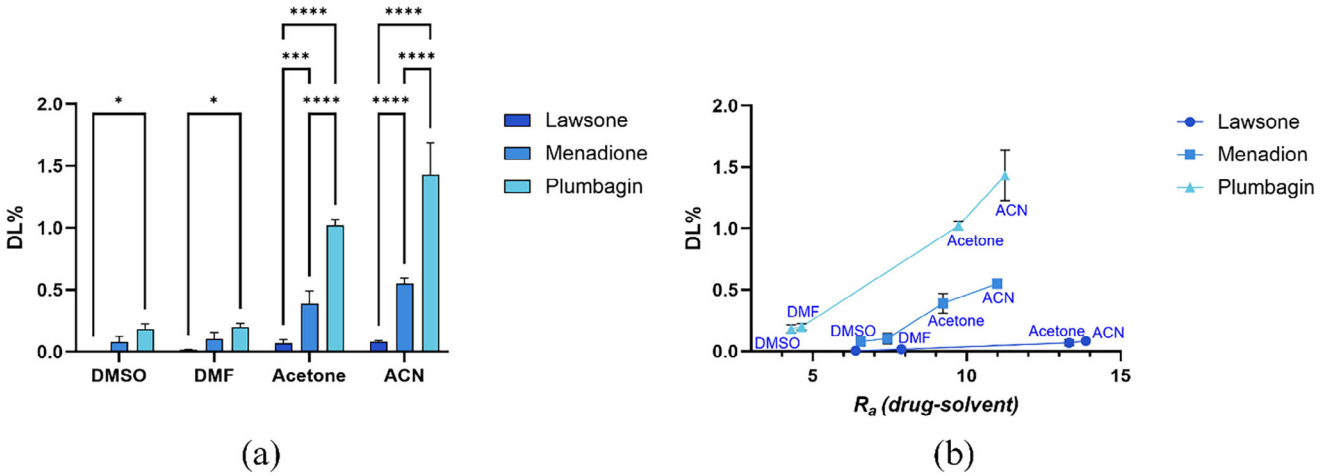

FIGURE 2 | (a) DL% of PLGA nanoparticles containing 1,4-naphthoquinone derivatives prepared using various organic solvents. (b) Correlation between DL and R_a between drug and solvent. *p <0.05, ***p <0.001, ****p <0.0001. All data displayed are mean values ± standard deviation from n = 3 independent experiments.

TABLE 2 | Z-average hydrodynamic diameters of PLGA nanoparticles and solvent-water affinity.

	Z-average (nm)			
Solvent phase	**Lawsone**	**Menadione**	**Plumbagin**	**R_a (solvent-water)**
DMSO	171.5 ± 1.0	126.4 ± 0.6	115.8 ± 4.9	32.6
DMF	196.3 ± 6.1	133.6 ± 4.4	126.6 ± 7.6	31.3
Acetone	211.5 ± 7.9	189.9 ± 1.6	171.3 ± 4.1	35.6
ACN	224.7 ± 12.0	195.1 ± 1.7	183.2 ± 3.5	36.3

affinity between solvent and non-solvent correlates with particle size; a higher affinity leads to smaller particles due to faster diffusion [58].

Table 2 shows the particle sizes of the drug-loaded PLGA particles and the affinity between water and organic solvent, expressed as R_a. The nanoparticles are spherical (Figure 3) and monodisperse (Figure 3; Table S2, PDI < 0.1) according to Hughes et al. [59], whereas ISO standard definitions consider a PDI of < 0.05 as the respective threshold [60, 61]. The z-averages range from 110 to 230 nm with zeta potentials ranging from −25 to −50 mV (Figure S4), indicating colloidal stability. As an orthogonal method for particle size determination, SEM analysis (Figure S2 and Table S1) yielded sizes that were in approximate agreement with the z-averages obtained by DLS. A similar trend is observed for each drug: particles prepared with DMSO and DMF are smaller than those prepared with acetone and ACN. This roughly correlates with the calculated R_a values; however, these values are substantially higher than those typically seen in polymer–solvent systems. This is due to water's exceptionally strong hydrogen bonding, which results in high polarity and complex, non-linear behavior (e.g., clustering and hydration shells) that cannot be reliably modeled by HSP models [62]. As such, HSPs may offer a general qualitative indication in this context but should not be used for quantitative predictions without experimental validation. This might also explain the general trend, but also the deviation for DMF and DMSO.

Another notable trend observed across all solvents was that particle sizes followed the order: lawsone > menadione > plumbagin (Figure 4). This observation suggests a correlation between particle size and drug loading, with smaller particles exhibiting higher drug loading. One possible explanation for this phenomenon is that a higher polymer-drug affinity shifts the ouzo region of the PLGA, as increased attractive interactions enhance the polymer's solubility in the solvent–nonsolvent system, leading to smaller particles [63]. The *ouzo effect* refers to the spontaneous formation of stable colloidal dispersions when a hydrophobic solute dissolved in a water-miscible solvent is mixed with water, and the boundaries of this region can be shifted by solute–polymer interactions [64]. In addition, it has been observed that unloaded (blank) nanoparticles exhibit significantly smaller sizes compared to drug-loaded particles (Figure S3), which is consistent with previous reports [65, 66]. Precipitated drug substances without polymer were also imaged by SEM (Figure S7) to confirm that the nanospheres in the formulations are not self-assembled drug particles, but polymeric nanoparticles containing the respective drug.

2.3 | Topographical Analysis of Polymeric Films Using AFM

The organic phase used for nanoprecipitation was also utilized to prepare polymer films, which were subsequently analyzed

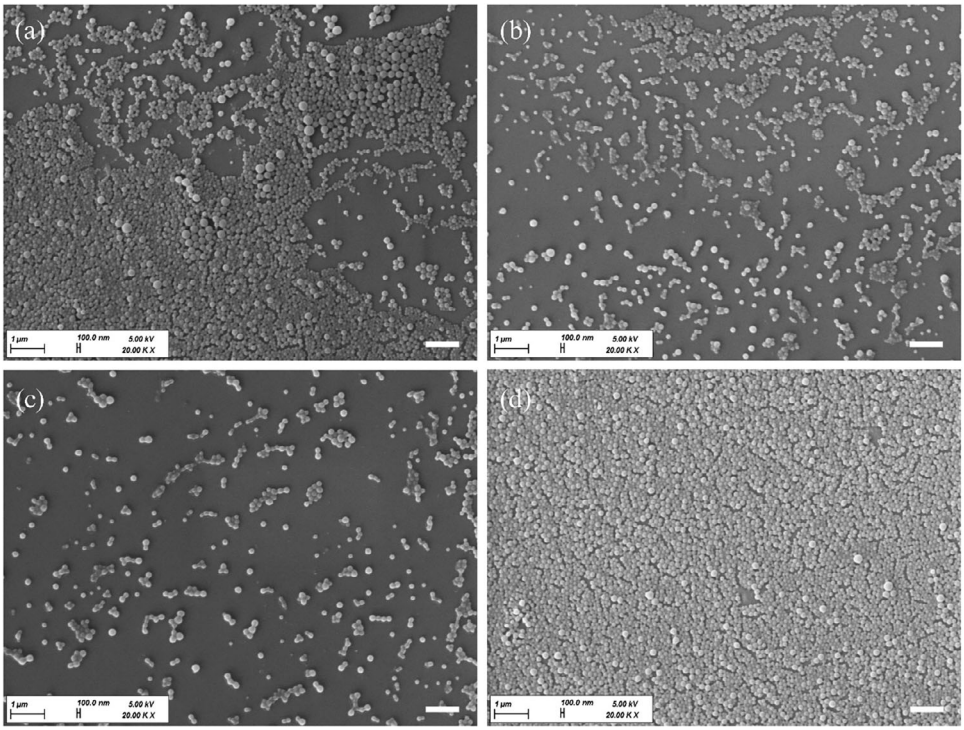

FIGURE 3 | SEM micrographs of PLGA nanoparticles: (a) plumbagin-loaded, (b) menadione-loaded, (c) lawsone-loaded, and (d) blank (unloaded). The nanoparticles were obtained using ACN as the organic phase with 5% w/w drug. Samples were prepared from a dispersion of the particles in the aqueous phase (MilliQ water). Scale bar: 1 μm.

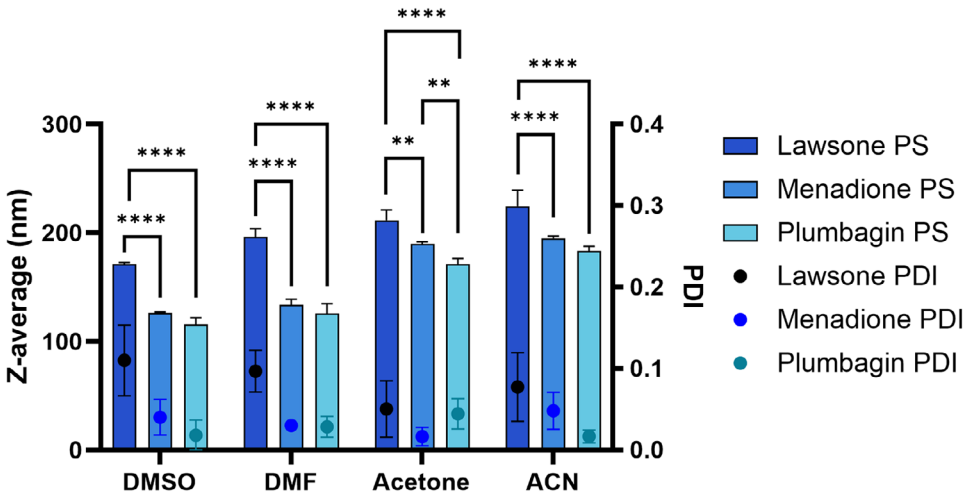

FIGURE 4 | Particle sizes (PS) of drug-loaded PLGA nanoparticles. $^{**}p < 0.01$, $^{****}p < 0.0001$. All data displayed are mean values ± standard deviation from $n = 3$ independent experiments.

by AFM (Figure 5a). Pore formation frequently occurs during solvent-based polymer film production [67]. The underlying mechanisms are attributed to phase separation processes, such as spinodal decomposition [68] and nucleation-and-growth, which are driven by solvent volatility, polymer–solvent miscibility, and drug–polymer interactions [69]. For the quantification of the porosity, threshold-based image analysis in ImageJ [70] was performed (Figure S6). Among the solvents tested—DMF, acetone, and ACN—films prepared with DMF showed the highest porosity, followed by those produced with acetone, while those prepared with ACN—films showed the lowest porosity (Figure 5b). DMSO was not tested because it does not evaporate enough, which prevented obtaining films of sufficient quality for quantitative determination of the polymer-covered area.

Solvent evaporation drives the phase separation of polymer films into distinct polymer-rich and polymer-lean domains, leading to dewetting and pore formation [68, 71, 72]. Additionally, the presence of different drug substances may further modulate the thermodynamic stability of the system, affecting miscibility and

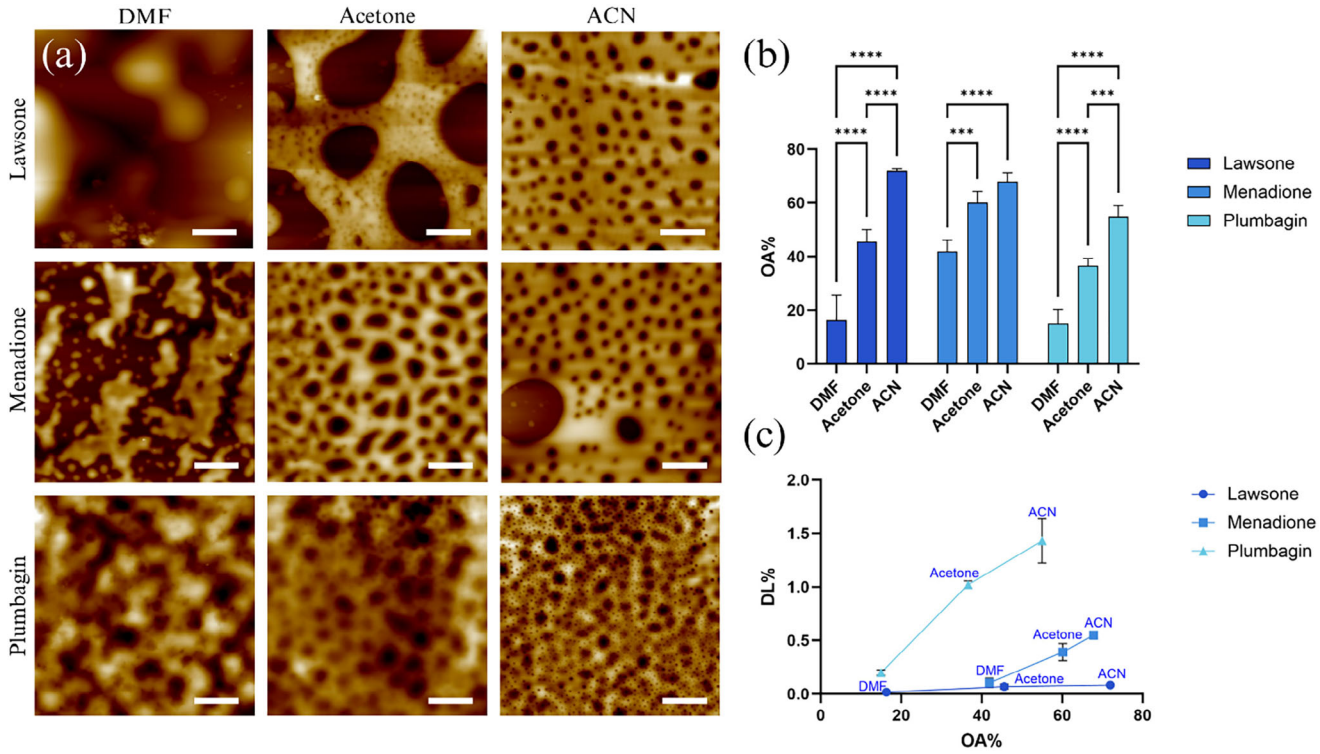

FIGURE 5 | (a) AFM micrographs of drug-loaded polymeric films prepared using DMF, acetone, and ACN as solvents. (b) Quantification of the polymer-covered area on the substrate (OA%). For each condition, OA% values were determined from three independent films, with one AFM image (50 × 50 μm) analyzed per film. (c) Correlation between DL% and OA% across all samples. ***p <0.001, ****p <0.0001. All data displayed are mean values ± standard deviation from $n = 3$ independent experiments. Scale bar: 10 μm.

TABLE 3 | *logP* values, HSPs, and R_a of lawsone, menadione, plumbagin, and PLGA.

	logP	δ_D	δ_P	δ_H	R_a
$PLGA_{50:50}$	n/a	17.4	11.0	8.0	
Lawsone	0.9 [74]	21.3	14.5	12.1	9.48
Menadione	2.2 [75]	20.0	12.3	6.2	5.65
Plumbagin	2.3 [76]	19.7	13.1	11.1	5.93

The HSPs of the compounds were calculated by Y-MB method, HSPs of PLGA were determined experimentally (Figure S8).

the kinetics of phase separation during film formation. This effect is supported by the measured OA% values, which correlate with DL% of the corresponding nanoparticles (Figure 5c), indicating that this AFM-based assay might be suitable as a prescreening method for drug loading. Blank films prepared with DMF and ACN exhibited no detectable pores, while acetone-based films showed only minor incipient porosity (Figure S5), confirming that pore formation is significantly influenced by the presence of drug substances.

2.4 | Assessment of Drug-Polymer Compatibility Using SEM

Drug–polymer compatibility can be estimated by calculating R_a (Table 3). Accordingly, Lawsone demonstrates the weakest affinity for PLGA, consistent with its low logP value and resulting hydrophilicity, while menadione and plumbagin showing comparatively stronger interactions. In this context, R_a is not a better indicator than logP, as both menadione and plumbagin have nearly identical logP values (2.2 and 2.3) and very similar R_a values (5.65 and 5.93), despite showing markedly different DL%. HSPs therefore provide only a rough estimate of drug-polymer miscibility but allow to better choose a certain solvent for improving drug loading. Beyond general solubility similarity (R_a), specific molecular interactions—particularly hydrogen bonding has been shown to significantly enhance drug loading in polymeric carriers [73]. The higher DL% of plumbagin compared to menadione may therefore be attributed, at least in part, to its higher δ_H value.

PLGA films containing varying drug concentrations (10%–50%) were prepared by solvent evaporation to assess drug-polymer compatibility using SEM. The estimation of drug-polymer compatibility was based on the assumption that each compound has a specific saturation threshold in the polymer matrix. When this threshold is exceeded, the excess drug cannot remain molecularly dispersed and separates out as crystalline or amorphous domains.

Needle-shaped crystalline precipitates are already observed in polymer films containing 10% w/w lawsone (Figure 6). For menadione, a distinct change in film morphology was observed starting at 20% w/w. At higher drug concentrations, needle-shaped, fiber-like precipitates became visible. For plumbagin, phase separation was observed at 30% w/w in the form of irregular shaped aggregates. This concentration-dependent behavior reflects the nanoparticle drug loading data (Figure 2a), with lawsone showing

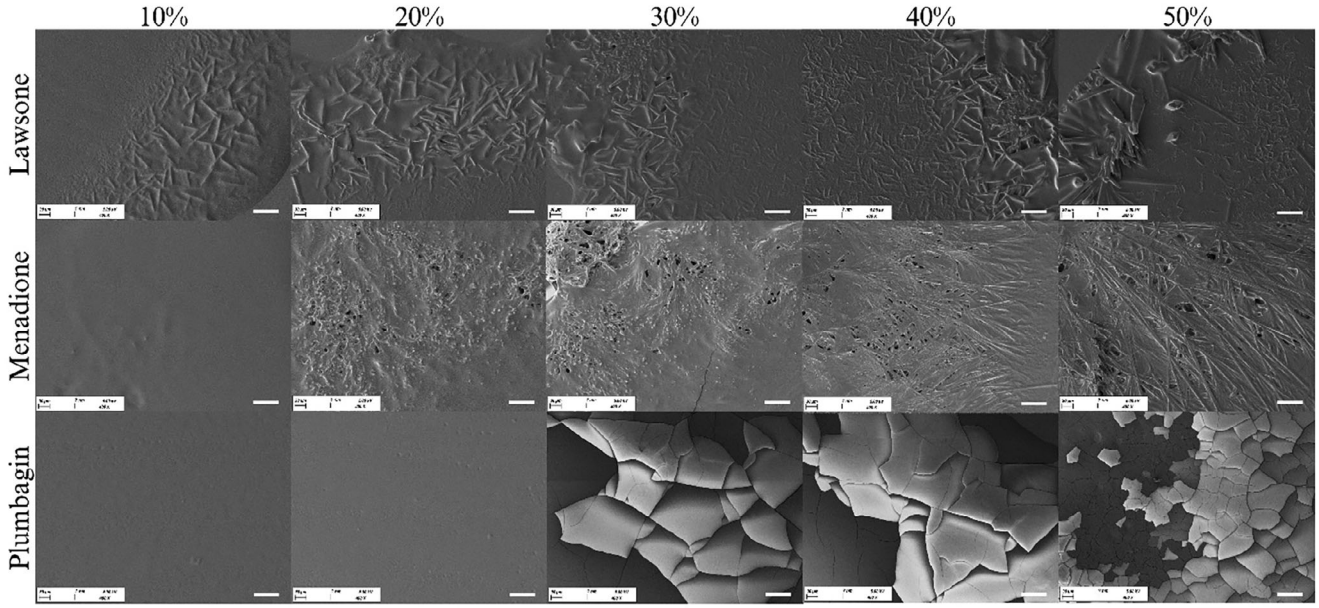

FIGURE 6 | SEM micrographs of PLGA films containing lawsone (top row), menadione (middle row), and plumbagin (bottom row). Scale bar: 60 μm.

the lowest loading, menadione intermediate, and plumbagin the highest. These observations highlight that this SEM analysis could serve as a useful prescreening tool for estimating polymer-drug compatibility in the context of nanoparticle formulation and provide comparative insight into loading capacities of different drugs in a given polymer matrix. Notably, the concentrations of drug substances used in this study are considerably higher than those used for the nanoparticle formulations. Solid dispersions like amorphous solid dispersions (ASDs), commonly achieve drug loadings in the range of 20%–50% w/w [77]. Reduced drug loadings in polymeric nanoparticles are largely a result of drug partitioning between the polymer and aqueous phases as well as diffusion losses during the purification process [66, 78]. Another factor limiting drug loading in polymeric nanoparticles is that drug incorporation is often kinetically driven; the rate at which the drug diffuses and co-precipitates with the polymer significantly affects encapsulation efficiency [9]. Nevertheless, the drug-polymer miscibility, which was determined in solid dispersions, can be correlated with the compatibility in nanoparticles [24]. These elevated concentrations were used to stress the polymer matrix and to make phase separation phenomena experimentally detectable. The results are therefore not intended to provide quantitative predictions of nanoparticle loading, but rather qualitative insights into relative drug–polymer miscibility. A limitation of this study is that it focused on a panel of structurally related naphthoquinones and a single polymer (PLGA). This design allowed us to establish proof-of-concept, but further studies using structurally diverse drug classes and polymers will be required to assess the broader applicability of our findings.

2.5 | Assessment of Drug-Polymer Compatibility Using DSC

Besides the interaction of the drug and the polymer with the solvent, drug-polymer interaction will contribute to the loading process. DSC is a common analytical technique to evaluate the compatibility between polymers and drug substances [52, 53, 79]. This technique offers various approaches like the zero-enthalpy extrapolation method [9, 80], melting point depression method [19, 24, 79], annealing method [81], and recrystallization method [82]. DSC-determined drug–polymer compatibility has been shown to correlate with nanoparticle drug loading, allowing it to serve as a predictive tool [9, 24, 83–85]. The zero-enthalpy extrapolation method relies on the premise that drug exceeding its solubility in the polymer matrix crystallizes and appears as a melting peak in DSC analysis. Accordingly, the solubility of the drug in the polymer matrix is defined as the concentration at which it no longer contributes to the melting enthalpy. This technique allows determination of solubility even near or below glass transition temperatures, where kinetic limitations often prevent accurate results for traditional methods (e.g., melting point depression method). It also provides a linear relationship between melting enthalpy and composition, enabling precise extrapolation to determine solubility. Additionally, it is reported to be valid for both high and low molecular weight systems, which can be applied to polymeric matrices and low molecular weight amorphous matrices, making it versatile for a variety of formulation systems [80]. A key limitation of this method is the assumption that excess drug substance precipitates as a crystalline phase. If the substance instead forms amorphous or metastable phases, solubility cannot be reliably determined. Another limitation common to all thermal analysis methods is the requirement for thermal stability: compounds must be stable upon melting and remain stable during annealing and scanning. Furthermore, since thermodynamic solubility below the glass transition temperature is not well defined, the method offers a semi-quantitative estimation of apparent drug solubility in the polymer rather than the true thermodynamic solubility, with a risk of overestimation. It should be noted that lawsone was excluded from DSC analysis because, unlike menadione and plumbagin, it lacks sufficient thermal stability and decomposes upon melting.

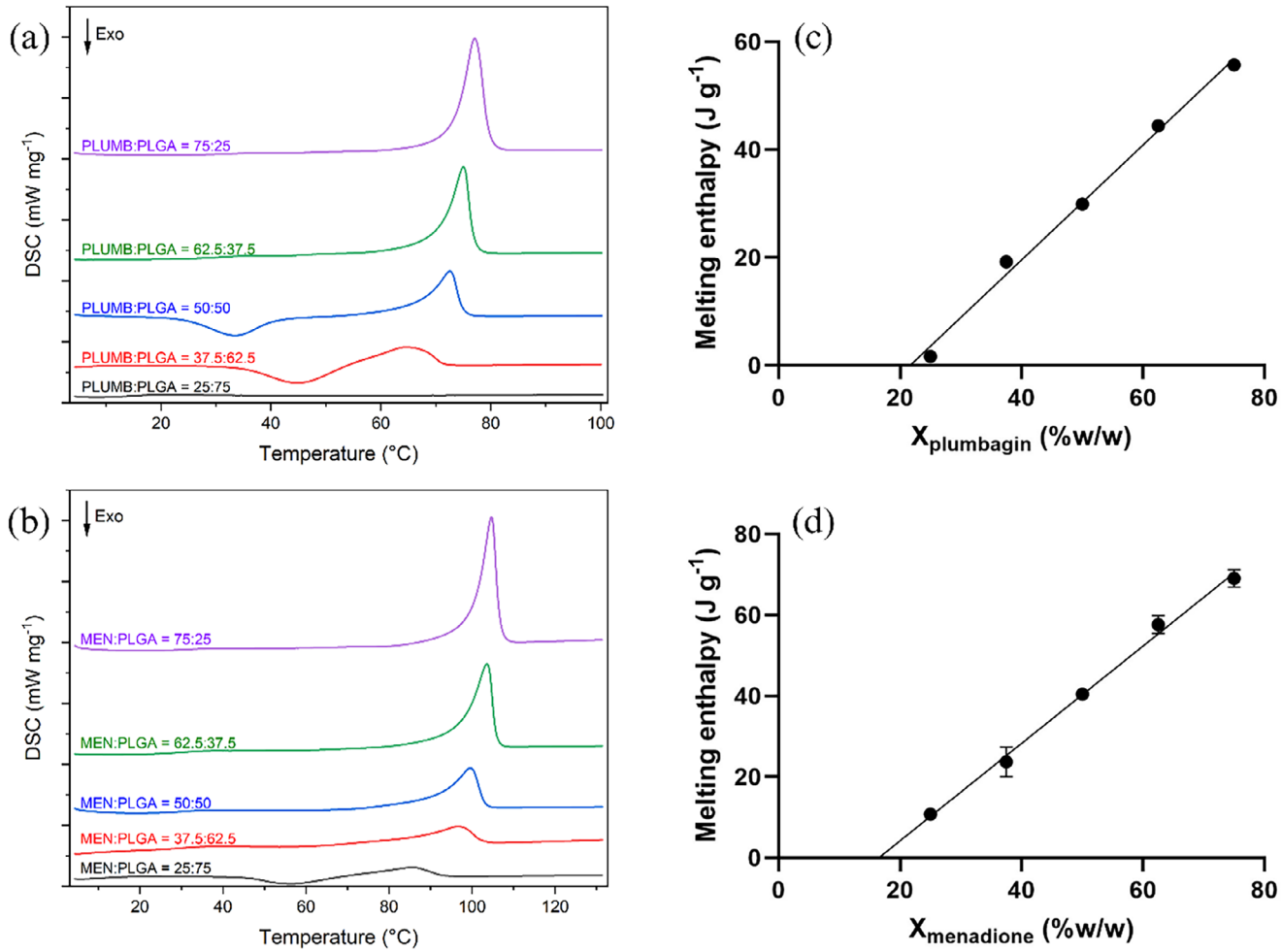

FIGURE 7 | DSC thermograms of drug-polymer blends (a) plumbagin, (b) menadione and plots of the melting enthalpy (c) plumbagin, (d) menadione.

TABLE 4 | Thermometric solubility data (DSC) of drug-PLGA matrices determined by the zero-enthalpy extrapolation method.

Drug	logP	Solubility of drug in PLGA matrix (% w/w)	Calculated SD of x_0
Menadione	2.2	16.52	1.44
Plumbagin	2.3	21.68	1.52

Thermograms for menadione and plumbagin containing PLGA matrices were successfully obtained, showing prominent melting peaks of the drug substances (Figure 7a,b). As expected, the melting enthalpy was observed to increase proportionally with the drug substance content. To determine the solubility of the drug substances in the PLGA matrix, the melting enthalpy was plotted against their mass fraction. The absolute solubility was then derived by extrapolation (Figure 7c,d). Plumbagin exhibited higher solubility in the polymer matrix (Table 4), consistent with its significantly greater drug loading in the nanoparticles; the calculated standard deviation of the x-axis intercept allows to estimate the variability of the extrapolated concentration threshold in the polymer. Thermally derived solubility data offer valuable information on drug–polymer affinity, which also appears to correlate with behavior in nanoparticle systems.

3 | Conclusion

PLGA nanoparticles of sizes ranging from 110 to 230 nm (PDI < 0.1) loaded with plumbagin, menadione, and lawsone were successfully prepared. The affinity between drug substances and solvents, expressed by R_a, significantly influences encapsulation and shows an almost linear correlation. Drug loading was also found to influence particle size, with higher loading resulting in comparatively smaller particles due to favorable intermolecular interactions. These interactions could be revealed by AFM enabling visualization of PLGA films' structure containing drug substances. Film morphology is strongly influenced by the choice of solvents and drug substances. The pronounced pore formation, which is driven by dewetting phenomena such as spinodal decomposition, can be quantified through graphical analysis and correlates with the drug loading of the corresponding nanoparticles. Drug-polymer compatibility was assessed using SEM. Phase separation was found to be concentration-dependent; the observed trends align with drug loading behavior of the nanoparticles. Those huge changes in film morphology were well-demonstrated by electron microscopy. It should be noted that the drug contents used in PLGA films (≥10% w/w) were intentionally higher than those achieved in the nanoparticle formulations (~1%–2% w/w). The purpose of the film studies was not to replicate absolute drug loading, but to stress the polymer matrix and

thereby reveal miscibility limits and phase separation phenomena that are not detectable at lower concentrations. Consequently, the results should be interpreted as qualitative indicators of relative drug–polymer compatibility rather than quantitative predictors of nanoparticle drug loading. Furthermore, DSC with zero-enthalpy extrapolation was used to determine the solubility of the active ingredients to enable a quantitative evaluation of drug-polymer affinity. The resulting solubilities correlated well with SEM observations and drug loading trends. Additionally, SEM enables rapid estimation of phase separation which correlates with the drug loading trends, as it allows for high-throughput imaging of multiple samples within a short time frame. The resulting data shows good correlation with values obtained via the zero-enthalpy method, which assesses drug-polymer solubility using DSC. The combined use of HSP-derived affinities, thin-film morphology, and solid-state solubility is best suited for screening and rank-ordering drug-polymer-solvent combinations prior to formulation, with trends aligning with observed DL%. Future work should expand this approach to structurally diverse drugs and alternative polymers to confirm the broader applicability of the observed correlations.

4 | Experimental Section

4.1 | Materials

Resomer 503H (Mw: 24,000-38,000 g mol^{-1}, Evonik), menadione (Sigma–Aldrich, Steinheim, Germany), plumbagin (98%, TCI, Eschborn, Germany), lawsone (98%, TCI), Poloxamer 407 (Caesar and Loretz GmbH, Hilden, Germany). ACN (HPLC grade), acetone (HPLC grade), DMF (analytical grade), DMSO (analytical grade) were purchased from Fischer Scientific (Schwerte, Germany).

4.2 | Calculation of HSPs and R_a

The HSPs were calculated using the Y-MB method, a refined group contribution approach using neural networks integrated into the HSPiP software (Hansen Solubility Parameters in Practice, version 5.4.03, Hansen-Solubility.com, UK). The parameters are δ_d, $\delta_{p,}$ and δ_h and can be combined to calculate the total solubility parameter, δ_t, by following formula:

$$\delta_t{}^2 = \delta_d{}^2 + \delta_p{}^2 + \delta_h{}^2 \quad (1)$$

The individual parameters represent the cohesive energy densities associated with interactions from dispersion forces, polar forces, and hydrogen bonding forces. The distances between two substances in the Hansen space are calculated by the following formula:

$$R_a{}^2 = 4(\delta_{d2} - \delta_{d1})^2 + \left(\delta_{p2} - \delta_{p1}\right)^2 + (\delta_{h2} - \delta_{h1})^2 \quad (2)$$

4.3 | Preparation of PLGA Nanoparticles

The nanoparticles were prepared using nanoprecipitation first described by Fessi et al. [86]. 25 mg PLGA was dissolved in 1.5 mL of an organic solvent (DMSO, DMF, acetone, or ACN) containing the drug substance (plumbagin, lawsone, or menadione) at a concentration of 5% relative to the polymer mass. The organic phase was injected into a stirred (750 rpm) 10 mL of 0.5% poloxamer 407 aqueous solution at a rate of 0.5 mL/min using a syringe pump (PHD 2000, Harvard Apparatus, Holliston, MA, United States). The samples were stirred overnight, leading to the complete evaporation of ACN and acetone, while DMSO and DMF remained largely in the suspension and were subsequently removed during the purification steps. The particles were purified through two centrifugation cycles (7500 × g, 20 min, 20°C), replacement of the supernatant with fresh MilliQ water, and resuspension. All formulations were prepared in triplicates.

4.4 | Characterization (Particle Size, PDI) of PLGA Nanoparticles

Particle size and zeta potential were measured using dynamic light scattering (DLS) and laser doppler electrophoresis (Zetasizer Ultra, Malvern Panalytical, Malvern, UK). Samples were diluted with 5 mM KCl to a nanoparticle concentration of approx. 0.125 mg/ml, and 1 mL was transferred into a zeta potential folded cuvette. The intensity-based measurements were conducted at 25°C at a detection angle of 173° in the backscattering mode. The zeta potential was based on electrophoretic migration and was performed at 25°C. All measurements were carried out in triplicates.

4.5 | Nanoparticle Morphology Using Scanning Electron Microscopy (SEM)

The nanoparticle suspension (20 µl, obtained from ACN as the organic phase and dispersed in MilliQ water) was applied onto a silica wafer fixed on an aluminum stub. After 2 min, the excess liquid was removed with compressed air. A thin gold layer (10 nm) was sputtered onto the sample (Quorum Q150R ES, Quorum Technologies, Laughton, UK) prior to imaging with the SEM (Zeiss EVO HD15, Carl Zeiss, Oberkochen, Germany).

4.6 | Morphology Analysis of Polymer Films Using Scanning Electron Microscopy (SEM)

The topography of the polymer films was analyzed using SEM. PLGA solutions (16.67 mg/mL in acetone) containing 10%–50% drug substance relative to the polymer content were prepared. A 20 µl aliquot of each solution was applied onto a silica wafer. After solvent evaporation (2 h), the polymer films were sputtered with a thin gold layer and then analyzed.

4.7 | Morphology Analysis of Polymer Films Using Atomic Force Microscopy (AFM)

For topography analysis, 50 µl of the organic phase, identical to that used for nanoparticle preparation, was applied to a mica substrate. The PLGA concentration was 16.67 mg/mL, and the drug concentration was 0.83 mg/mL with acetonitrile, acetone, and DMF used as solvents. After overnight evapora-

tion, the sample was then visualized in Tapping Mode using a OMCL-AC160TS cantilever (Bruker, Wissembourg, France) with a BioScope (Veeco, Santa Barbara, CA, USA). Images of 50x50 µm were taken and the occupied area was quantified through binary image processing in ImageJ (version 1.54m, NIH, Bethesda, MD, USA).

4.8 | Thermometric Analysis of Polymer-Drug Blends

Polymer-drug blends were prepared by dissolving PLGA and the drug substances (menadione, plumbagin) in various ratios (0.25, 0.375, 0.5, 0.625 and 0.75) in acetone, followed by solvent evaporation at room temperature. Thermal properties were analyzed using DSC 204 F1 Phoenix calorimeter (NETZSCH-Gerätebau GmbH, Selb, Germany) with a nitrogen flow of 100 mL/min and a heating rate of 10 K/min. Three cycles were run for each measurement with the second used for data evaluation. The data was analyzed using NETZSCH Proteus—Thermal Analysis software (version 5.2.0, NETZSCH-Gerätebau GmbH, Selb, Germany). The solubility of the active ingredients in the polymer matrix was determined using the zero-enthalpy extrapolation method [9, 80, 87].

4.9 | DL% Determination

An aliquot was taken from the nanoparticle suspension and washed twice by centrifugation (40,000 × g, 30 min, 20°C). After each cycle, the supernatant was removed, and the pellet was resuspended with fresh MilliQ water. Following the second centrifugation cycle, the pellet was frozen at −80°C and lyophilized overnight. Dry pellet masses were determined on a microbalance (Sartorius AG, Göttingen, Germany). The pellets were dissolved in ACN, and the drug substances were directly quantified by absorbance measurement ($\lambda = 254$ nm) using UV-Star 96-well F-bottom plates (Greiner Bio-One, Frickenhausen, Germany) and a microplate reader (Infinite M200, Tecan Group, Männedorf, Switzerland).

4.10 | Data Evaluation and Statistics

Statistical significance was assessed using one-way or two-way analysis of variance (ANOVA), depending on the number of independent variables, followed by Tukey's post-hoc test for pairwise comparisons. A p-value of <0.05 was considered significant. All analyses were performed using GraphPad Prism software (version 10.4.2, GraphPad Software, 2025).

Acknowledgements

The authors would like to thank Pascal Paul (Helmholtz Institute for Pharmaceutical Research Saarland) for the support with the SEM analysis.

Open access funding enabled and organized by Projekt DEAL.

Conflicts of Interest

The authors declare no conflicts of interest.

Data Availability Statement

The data that support the findings of this study are available from the corresponding author upon reasonable request.

References

1. L. M. D. A. C. Gaspar, A. C. S. Dórea, D. Droppa-Almeida, et al., "Development and Characterization of PLGA Nanoparticles Containing Antibiotics," *Journal of Nanoparticle Research* 20, no. 11 (2018): 289, https://doi.org/10.1007/s11051-018-4387-z.

2. E. Lagreca, V. Onesto, C. Di Natale, S. La Manna, P. A. Netti, and R. Vecchione, "Recent Advances in the Formulation of PLGA Microparticles for Controlled Drug Delivery," *Progress in Biomaterials* 9, no. 4 (2020): 153–174, https://doi.org/10.1007/s40204-020-00139-y.

3. A. Zielińska, F. Carreiró, A. M. Oliveira, et al., "Polymeric Nanoparticles: Production, Characterization, Toxicology and Ecotoxicology," *Molecules (Basel, Switzerland)* 25, no. 16 (2020): 3731.

4. A. K. Shah and S. A. Agnihotri, "Recent Advances and Novel Strategies in Pre-clinical Formulation Development: an Overview," *Journal of Controlled Release* 156, no. 3 (2011): 281–296, https://doi.org/10.1016/j.jconrel.2011.07.003.

5. N. Wang, X. Cheng, N. Li, H. Wang, and H. Chen, "Nanocarriers and Their Loading Strategies," *Advanced Healthcare Materials* 8, no. 6 (2019): 1801002, https://doi.org/10.1002/adhm.201801002.

6. M. H. Stenzel, "The Trojan Horse Goes Wild: The Effect of Drug Loading on the Behavior of Nanoparticles," *Angewandte Chemie International Edition* 60, no. 5 (2021): 2202–2206, https://doi.org/10.1002/anie.202010934.

7. A. Judefeind and M. M. de Villiers, "*Drug Loading into and in Vitro Release from Nanosized Drug Delivery Systems, in Nanotechnology in Drug Delivery*," ed. M. V. Melgardt, P. Aramwit, and G. S. Kwon (Springer, 2009), 129–162, https://doi.org/10.1007/978-0-387-77667-5.

8. E. Piacentini, "*Encapsulation Efficiency, in Encyclopedia of Membranes*," ed. E Drioli and L Giorno, (Springer, 2016), 706–707.

9. S. I. Hamdallah, R. Zoqlam, B. Yang, et al., "Using a Systematic and Quantitative Approach to Generate New Insights into Drug Loading of PLGA Nanoparticles Using Nanoprecipitation," *Nanoscale Advances* 6, no. 12 (2024): 3188–3198, https://doi.org/10.1039/d4na00087k.

10. C. J. Martínez Rivas, M. Tarhini, W. Badri, et al., "Nanoprecipitation Process: From Encapsulation to Drug Delivery," *International Journal of Pharmaceutics* 532, no. 1 (2017): 66–81, https://doi.org/10.1016/j.ijpharm.2017.08.064.

11. I. J. Joye and D. J. McClements, "Production of Nanoparticles by Anti-Solvent Precipitation for Use in Food Systems," *Trends in Food Science & Technology* 34, no. 2 (2013): 109–123, https://doi.org/10.1016/j.tifs.2013.10.002.

12. Y. Liu, G. Yang, D. Zou, et al., "Formulation of Nanoparticles Using Mixing-Induced Nanoprecipitation for Drug Delivery," *Industrial & Engineering Chemistry Research* 59, no. 9 (2020): 4134–4149, https://doi.org/10.1021/acs.iecr.9b04747.

13. A. J. Zander, M.-S. Ehrlich, S. Rehman, and M. Schneider, "Evaporation-Triggered Nanoprecipitation for PLGA Nanoparticle Formation Using a Spinning-Disc System," *Journal of Drug Delivery Science and Technology* 108 (2025): 106901, https://doi.org/10.1016/j.jddst.2025.106901.

14. S. A. Khan and M. Schneider, "Stabilization of Gelatin Nanoparticles without Crosslinking," *Macromolecular Bioscience* 14, no. 11 (2014): 1627–1638, https://doi.org/10.1002/mabi.201400214.

15. M. Beck-Broichsitter, "Solvent Impact on Polymer Nanoparticles Prepared Nanoprecipitation," *Colloids and Surfaces A: Physicochemical and Engineering Aspects* 625 (2021): 126928, https://doi.org/10.1016/j.colsurfa.2021.126928.

16. M. Chorny, I. Fishbein, H. D. Danenberg, and G. Golomb, "Lipophilic Drug Loaded Nanospheres Prepared by Nanoprecipitation: Effect of Formulation Variables On Size, Drug Recovery and Release Kinetics," *Journal of Controlled Release* 83, no. 3 (2002): 389–400, https://doi.org/10.1016/S0168-3659(02)00211-0.

17. A. Budhian, S. J. Siegel, and K. I. Winey, "Haloperidol-Loaded PLGA Nanoparticles: Systematic Study of Particle Size and Drug Content," *International Journal of Pharmaceutics* 336, no. 2 (2007): 367–375, https://doi.org/10.1016/j.ijpharm.2006.11.061.

18. Y. Dong and S.-S. Feng, "Methoxy Poly(Ethylene Glycol)-Poly(Lactide) (MPEG-PLA) Nanoparticles for Controlled Delivery of Anticancer Drugs," *Biomaterials* 25, no. 14 (2004): 2843–2849, https://doi.org/10.1016/j.biomaterials.2003.09.055.

19. S. Liu, M. Li, L. Jia, et al., "Investigation of Drug–Polymer Miscibility, Molecular Interaction, and Their Effects on the Physical Stabilities and Dissolution Behaviors of Norfloxacin Amorphous Solid Dispersions," *Crystal Growth and Design* 20, no. 5 (2020): 2952–2964, https://doi.org/10.1021/acs.cgd.9b01571.

20. M. Meunier, A. Goupil, and P. Lienard, "Predicting Drug Loading in PLA-PEG Nanoparticles," *International Journal of Pharmaceutics* 526, no. 1-2 (2017): 157–166, https://doi.org/10.1016/j.ijpharm.2017.04.043.

21. J. Ghitman, R. Stan, G. Vlasceanu, E. Vasile, and H. Iovu, "Predicting the Drug Loading Efficiency Into Hybrid Nanocarriers Based on PLGA-vegetable Oil Using Molecular Dynamic Simulation Approach and Flory-Huggins Theory," *Journal of Drug Delivery Science and Technology* 53 (2019): 101203, https://doi.org/10.1016/j.jddst.2019.101203.

22. M. Murase and R. Ohta, "Prediction of Molecular Affinity on Solid Surfaces via Three-Dimensional Solubility Parameters Using Interfacial Free Energy as Interaction Threshold," *The Journal of Physical Chemistry C* 123, no. 21 (2019): 13246–13252, https://doi.org/10.1021/acs.jpcc.9b00154.

23. C. G. Madsen, A. Skov, S. Baldursdottir, T. Rades, L. Jorgensen, and N. J. Medlicott, "Simple Measurements for Prediction of Drug Release from Polymer Matrices—Solubility Parameters and Intrinsic Viscosity," *European Journal of Pharmaceutics and Biopharmaceutics* 92 (2015): 1–7, https://doi.org/10.1016/j.ejpb.2015.02.001.

24. Y. Niyom, D. Crespy, and A. E. Flood, "Compatibility between Drugs and Polymer in Nanoparticles Produced by the Miniemulsion-Solvent Evaporation Technique," *Macromolecular Materials and Engineering* 306, no. 7 (2021): 2100102, https://doi.org/10.1002/mame.202100102.

25. E. Stefanis and C. Panayiotou, "Prediction of Hansen Solubility Parameters with a New Group-Contribution Method," *International Journal of Thermophysics* 29, no. 2 (2008): 568–585, https://doi.org/10.1007/s10765-008-0415-z.

26. H. W. Milliman, D. Boris, and D. A. Schiraldi, "Experimental Determination of Hansen Solubility Parameters for Select POSS and Polymer Compounds as a Guide to POSS–Polymer Interaction Potentials," *Macromolecules* 45, no. 4 (2012): 1931–1936, https://doi.org/10.1021/ma202685j.

27. A. Erlebach, T. Ott, C. Otzen, et al., "Thermodynamic compatibility of actives encapsulated Into PEG-PLA nanoparticles: In Silic o predictions and experimental verification," *Journal of Computational Chemistry* 37, no. 24 (2016): 2220–2227, https://doi.org/10.1002/jcc.24449.

28. R. Mackenzie, J. Booth, C. Alexander, M. C. Garnett, and C. A. Laughton, "Multiscale Modeling of Drug–Polymer Nanoparticle Assembly Identifies Parameters Influencing Drug Encapsulation Efficiency," *Journal of Chemical Theory and Computation* 11, no. 6 (2015): 2705–2713, https://doi.org/10.1021/ct501152a.

29. I. Muljajew, M. Chi, A. Vollrath, et al., "A Combined Experimental and in Silico Approach to Determine the Compatibility of Poly(ester amide)s and Indomethacin in Polymer Nanoparticles," *European Polymer Journal* 156 (2021): 110606, https://doi.org/10.1016/j.eurpolymj.2021.110606.

30. J. Kehrein, A. Bunker, and R. Luxenhofer, "POxload: Machine Learning Estimates Drug Loadings of Polymeric Micelles," *Molecular Pharmaceutics* 21, no. 7 (2024): 3356–3374, https://doi.org/10.1021/acs.molpharmaceut.4c00086.

31. K. Miladi, S. Sfar, H. Fessi, and A. Elaissari, "*Nanoprecipitation Process: from Particle Preparation to in Vivo Applications, in Polymer Nanoparticles for Nanomedicines: a Guide for Their Design, Preparation and Development*,"ed. C Vauthier and G Ponchel, (Springer 2016), 17–53.

32. J. Khan, A. Rani, M. Aslam, G. Pandey, and B. N. Pant, "A Review on the Synthesis and Application of Naphthoquinone-based Drugs," *Results in Chemistry* 6 (2023): 101138, https://doi.org/10.1016/j.rechem.2023.101138.

33. S. Padhye, P. Dandawate, M. Yusufi, A. Ahmad, and F. H. Sarkar, "Perspectives on Medicinal Properties of plumbagin and Its Analogs," *Medicinal Research Reviews* 32, no. 6 (2012): 1131–1158, https://doi.org/10.1002/med.20235.

34. L. B. Negri, Y. Mannaa, S. Korupolu, W. A. Farinelli, R. R. Anderson, and J. A. Gelfand, "Vitamin K3 (Menadione) Is a Multifunctional Microbicide Acting as a Photosensitizer and Synergizing with Blue Light to Kill Drug-resistant Bacteria in Biofilms," *Journal of Photochemistry and Photobiology B: Biology* 244 (2023): 112720, https://doi.org/10.1016/j.jphotobiol.2023.112720.

35. A. Singh, A. Basu, A. Sharma, et al., "Lawsone (2-hydroxy-1,4-naphthaquinone) Derived Anticancer Agents," *Physical Sciences Reviews* 8, no. 10 (2023): 2967–2994, https://doi.org/10.1515/psr-2021-0043.

36. K. Shehu, M. Schneider, and A. Kraegeloh, "Menadione as Antibiotic Adjuvant Against P. aeruginosa: Mechanism of Action, Efficacy and Safety," *Antibiotics* 14, no. 2 (2025): 163.

37. E. L. J. Moya, S. M. Lombardo, E. Vandenhaute, et al., "Interaction of Surfactant Coated PLGA Nanoparticles with in Vitro human Brain-Like Endothelial Cells," *International Journal of Pharmaceutics* 621 (2022): 121780, https://doi.org/10.1016/j.ijpharm.2022.121780.

38. N. Lababidi, V. Sigal, A. Koenneke, et al., "Microfluidics as Tool to Prepare Size-tunable PLGA Nanoparticles with High Curcumin Encapsulation for Efficient Mucus Penetration," *Beilstein Journal of Nanotechnology* 10 (2019): 2280–2293, https://doi.org/10.3762/bjnano.10.220.

39. H. K. Makadia and S. J. Siegel, "Poly Lactic-co-Glycolic Acid (PLGA) as Biodegradable Controlled Drug Delivery Carrier," *Polymers* 3, no. 3 (2011): 1377–1397.

40. A. M. Joshua, G. Cheng, and E. V. Lau, "Soft Matter Analysis via Atomic Force Microscopy (AFM): a Review," *Applied Surface Science Advances* 17 (2023): 100448, https://doi.org/10.1016/j.apsadv.2023.100448.

41. M. S. Ural, E. Dartois, J. Mathurin, et al., "Quantification of Drug Loading in Polymeric Nanoparticles Using AFM-IR Technique: a Novel Method to Map and Evaluate Drug Distribution in Drug Nanocarriers," *The Analyst* 147, no. 23 (2022): 5564–5578, https://doi.org/10.1039/d2an01079h.

42. P. Nguyen-Tri, P. Ghassemi, P. Carriere, S. Nanda, A. A. Assadi, and D. D. Nguyen, "Recent Applications of Advanced Atomic Force Microscopy in Polymer Science: a Review," *Polymers* 12, no. 5 (2020): 1142, https://doi.org/10.3390/polym12051142.

43. M. D. Timotijević, T. Ilić, B. Marković, et al., "Coupling AFM, DSC and FT-IR towards Elucidation of Film-Forming Systems Transformation to Dermal Films: a Betamethasone Dipropionate Case Study," *International Journal of Molecular Sciences* 23, no. 11 (2022): 6013, https://doi.org/10.3390/ijms23116013.

44. A.-V. Weiss, D. Schorr, J. K. Metz, M. Yildirim, S. A. Khan, and M. Schneider, "Gelatin Nanoparticles with Tunable Mechanical Properties: Effect of Crosslinking Time and Loading," *Beilstein Journal of Nanotechnology* 13 (2022): 778–787, https://doi.org/10.3762/bjnano.13.68.

45. A. K. Bajpai, R. Bhatt, and R. Katare, "Atomic Force Microscopy Enabled Roughness Analysis of Nanostructured Poly (diaminonaphthalene) Doped Poly (vinyl alcohol) Conducting Polymer Thin Films," *Micron (Oxford, England: 1993)* 90 (2016): 12–17, https://doi.org/10.1016/j.micron.2016.07.012.

46. B. Fang, W. Huang, Y. Luo, L. Xie, and T. Gu, "Quantitative Characterization of Surface Topography Using an Improved Deterministic Method," *Tribology Letters* 72, no. 4 (2024): 131, https://doi.org/10.1007/s11249-024-01932-7.

47. N. Rodriguez, L. Gontard, C. Ma, R. Xu, and B. N. J. Persson, "On How to Determine Surface Roughness Power Spectra," *Tribology Letters* 73, no. 1 (2024): 18, https://doi.org/10.1007/s11249-024-01933-6.

48. R. Pervin, P. Ghosh, and M. G. Basavaraj, "Tailoring Pore Distribution in Polymer Films *via* Evaporation Induced Phase Separation," *RSC Advances* 9, no. 27 (2019): 15593–15605, https://doi.org/10.1039/c9ra01331h.

49. F. Qian, J. Huang, and M. A. Hussain, "Drug-Polymer Solubility and Miscibility: Stability Consideration and Practical Challenges in Amorphous Solid Dispersion Development," *Journal of Pharmaceutical Sciences* 99, no. 7 (2010):2941–2947, https://doi.org/10.1002/jps.22074.

50. C. Hu, Q. Yan, Y. Zhang, and H. Yan, "Influence Mechanism of Drug–Polymer Compatibility on Humidity Stability of Crystalline Solid Dispersion," *Pharmaceuticals* 16, no. 12 (2023): 1640, https://doi.org/10.3390/ph16121640.

51. D. Medarević, J. Djuriš, P. Barmpalexis, K. Kachrimanis, and S. Ibrić, "Analytical and Computational Methods for the Estimation of Drug-Polymer Solubility and Miscibility in Solid Dispersions Development," *Pharmaceutics* 11, no. 8 (2019): 372, https://doi.org/10.3390/pharmaceutics11080372.

52. A. Mathers, F. Hassouna, M. Klajmon, and M. Fulem, "Comparative Study of DSC-Based Protocols for API–Polymer Solubility Determination," *Molecular Pharmaceutics* 18, no. 4 (2021): 1742–1757, https://doi.org/10.1021/acs.molpharmaceut.0c01232.

53. M. B. Rask, M. M. Knopp, N. E. Olesen, R. Holm, and T. Rades, "Comparison of Two DSC-Based Methods to Predict Drug-Polymer Solubility," *International Journal of Pharmaceutics* 540, no. 1 (2018): 98–105, https://doi.org/10.1016/j.ijpharm.2018.02.002.

54. E. Sah and H. Sah, "Recent Trends in Preparation of Poly(Lactide–Co–Glycolide) Nanoparticles by Mixing Polymeric Organic Solution With Antisolvent," *Journal of Nanomaterials* 2015, no. 1 (2015): 794601, https://doi.org/10.1155/2015/794601.

55. A. Kumari, S. K. Yadav, and S. C. Yadav, "Biodegradable Polymeric Nanoparticles Based Drug Delivery Systems," *Colloids and Surfaces B: Biointerfaces* 75, no. 1 (2010): 1–18, https://doi.org/10.1016/j.colsurfb.2009.09.001.

56. S. Abbott, C. M. Hansen, and Yamamoto *Hansen Solubility Parameters in Practice* (Hansen-Solubility 2015).

57. M. Kuddushi, C. Kanike, B. B. Xu, and X. Zhang, "Recent Advances in Nanoprecipitation: from Mechanistic Insights to Applications in Nanomaterial Synthesis," *Soft Matter* 21, no. 15 (2025): 2759–2781, https://doi.org/10.1039/D5SM00006H.

58. S. Galindo-Rodriguez, E. Allémann, H. Fessi, and E. Doelker, "Physicochemical Parameters Associated with Nanoparticle Formation in the Salting-Out, Emulsification-Diffusion, and Nanoprecipitation Methods," *Pharmaceutical Research* 21, no. 8 (2004): 1428–1439, https://doi.org/10.1023/B:PHAM.0000036917.75634.be.

59. J. M. Hughes, P. M. Budd, A. Grieve, P. Dutta, K. Tiede, and J. Lewis, "Highly Monodisperse, Lanthanide-Containing Polystyrene Nanoparticles as Potential Standard Reference Materials for Environmental "Nano" Fate Analysis," *Journal of Applied Polymer Science* 132, no. 24 (2015), https://doi.org/10.1002/app.42061.

60. Standardization, I.O.f. 1996. Particle size analysis — Photon correlation spectroscopy, ISO Standard 13321.

61. Standardization, I.O.f. 2008. Particle size analysis — Dynamic light scattering (DLS), ISO Standard 22412.

62. G. M. Kontogeorgis, A. Holster, N. Kottaki, et al., "Water Structure, Properties and Some Applications—A Review," *Chemical Thermodynamics and Thermal Analysis* 6 (2022): 100053, https://doi.org/10.1016/j.ctta.2022.100053.

63. M. Beck-Broichsitter, E. Rytting, T. Lebhardt, X. Wang, and T. Kissel, "Preparation of Nanoparticles by Solvent Displacement for Drug Delivery: a Shift in the "Ouzo Region" Upon Drug Loading," *European Journal of Pharmaceutical Sciences* 41, no. 2 (2010): 244–253, https://doi.org/10.1016/j.ejps.2010.06.007.

64. E. Lepeltier, C. Bourgaux, and P. Couvreur, "Nanoprecipitation and the "Ouzo Effect": Application to Drug Delivery Devices," *Advanced Drug Delivery Reviews* 71 (2014): 86–97, https://doi.org/10.1016/j.addr.2013.12.009.

65. S. Derman, "Caffeic Acid Phenethyl Ester Loaded PLGA Nanoparticles: Effect of Various Process Parameters on Reaction Yield, Encapsulation Efficiency, and Particle Size," *Journal of Nanomaterials* 2015, no. 1 (2015): 341848, https://doi.org/10.1155/2015/341848.

66. J. Xu, S. Zhang, A. Machado, et al., "Controllable Microfluidic Production of Drug-Loaded PLGA Nanoparticles Using Partially Water-Miscible Mixed Solvent Microdroplets as a Precursor," *Scientific Reports* 7, no. 1 (2017): 4794, https://doi.org/10.1038/s41598-017-05184-5.

67. H. Manzanarez, J. P. Mericq, P. Guenoun, and D. Bouyer, "Modeling the Interplay Between Solvent Evaporation and Phase Separation Dynamics During Membrane," *Journal of Membrane Science* 620 (2021): 118941, https://doi.org/10.1016/j.memsci.2020.118941.

68. J. Becker, G. Grün, R. Seemann, et al., "Complex Dewetting Scenarios Captured by Thin-Film Models," *Nature Materials* 2, no. 1 (2003): 59–63, https://doi.org/10.1038/nmat788.

69. V.-N. Tran Duc and P. K. Chan, "Using the Cahn-Hilliard Theory in Metastable Binary Solutions," *ChemEngineering* 3, no. 3 (2019): 75, https://doi.org/10.3390/chemengineering3030075.

70. C. A. Schneider, W. S. Rasband, and K. W. Eliceiri, "NIH Image to ImageJ: 25 Years of Image Analysis," *Nature Methods* 9, no. 7 (2012): 671–675, https://doi.org/10.1038/nmeth.2089.

71. D. Roy, S. Mandal, K. Chandrakar, and M. Dwivedi, "Controlling Porosity and Multifunctionality in Electrospun Polymeric Fibers by Nanoscale Phase Separations: Flory-Huggins Interaction Parameters Revisited," *Macromolecular Chemistry and Physics* 226, no. 13 (2025): 2500046, https://doi.org/10.1002/macp.202500046.

72. J. X. Liu, N. Bizmark, D. M. Scott, et al., "Evolution of Polymer Colloid Structure during Precipitation and Phase Separation," *JACS Au* 1, no. 7 (2021): 936–944, https://doi.org/10.1021/jacsau.1c00110.

73. X. Qu, J. Li, Y. Yu, and J. Yang, "Hydrogen Bonding Enhanced Drug-Polymer Interaction for Efficient Drug Loading and Delivery," *Soft Matter* 20, no. 16 (2024): 3387–3391, https://doi.org/10.1039/D4SM00003J.

74. Information, N.C.f.B. PubChem Compound Summary for CID 6755.

75. Information, N.C.f.B. PubChem Compound Summary for CID 4055.

76. Information, N.C.f.B. PubChem Compound Summary for CID 10205.

77. C. L.-N. Vo, C. Park, and B.-J. Lee, "Current Trends and Future Perspectives of Solid Dispersions Containing Poorly Water-soluble Drugs," *European Journal of Pharmaceutics and Biopharmaceutics* 85, no. 3 (2013): 799–813, https://doi.org/10.1016/j.ejpb.2013.09.007.

78. S. F. Tehrani, A. Garcia AC, M. A. Minani Tuyaga, T. Rode Garcia, X. Banquy, and V. G. Roullin, "Critical Assessment of Purification Processes for the Robust Production of Polymeric Nanomedicine," *International Journal of Pharmaceutics* 668 (2025): 124975, https://doi.org/10.1016/j.ijpharm.2024.124975.

79. C. Johnson and F. Zhang, "Development of a Melting Point Depression Method to Measure the Solubility of a Small-Molecule Drug in Poly-Lactic-Co-Glycolic Acid (PLGA)," *Pharmaceutical Research* 42, no. 3 (2025): 529–543, https://doi.org/10.1007/s11095-025-03840-4.

80. Y. Amharar, V. Curtin, K. H. Gallagher, and A. M. Healy, "Solubility of Crystalline Organic Compounds in High and Low Molecular Weight Amorphous Matrices above and below the Glass Transition by Zero Enthalpy Extrapolation," *International Journal of Pharmaceutics* 472, no. 1 (2014): 241–247, https://doi.org/10.1016/j.ijpharm.2014.06.038.

81. Z. Wei, P. Song, C. Zhou, et al., "Insight Into the Annealing Peak and Microstructural Changes of Poly(l-Lactic Acid) by Annealing at Elevated Temperatures," *Polymer* 54, no. 13 (2013): 3377–3384, https://doi.org/10.1016/j.polymer.2013.04.027.

82. M. M. Knopp, L. Tajber, Y. Tian, et al., "Comparative Study of Different Methods for the Prediction of Drug-Polymer Solubility," *Molecular Pharmaceutics* 12, no. 9 (2015): 3408–3419, https://doi.org/10.1021/acs.molpharmaceut.5b00423.

83. J. Panyam, D. Williams, A. Dash, D. Leslie-Pelecky, and V. Labhasetwar, "Solid-State Solubility Influences Encapsulation and Release of Hydrophobic Drugs From PLGA/PLA Nanoparticles," *Journal of Pharmaceutical Sciences* 93, no. 7 (2004): 1804–1814, https://doi.org/10.1002/jps.20094.

84. S. Dimiou, J. McCabe, R. Booth, et al., "Selecting Counterions to Improve Ionized Hydrophilic Drug Encapsulation in Polymeric Nanoparticles," *Molecular Pharmaceutics* 20, no. 2 (2023): 1138–1155, https://doi.org/10.1021/acs.molpharmaceut.2c00855.

85. G. Nabar, K. Mahajan, M. Calhoun, et al., "Micelle-Templated, Poly(Lactic-Co-Glycolic Acid) Nanoparticles for Hydrophobic Drug Delivery," *International Journal of Nanomedicine* 13 (2018): 351–366, https://doi.org/10.2147/ijn.s142079.

86. H. Fessi, F. Puisieux, J. P. Devissaguet, N. Ammoury, and S. Benita, "Nanocapsule Formation by Interfacial Polymer Deposition Following Solvent Displacement," *International Journal of Pharmaceutics* 55, no. 1 (1989): R1–R4, https://doi.org/10.1016/0378-5173(89)90281-0.

87. S. Qi, P. Belton, K. Nollenberger, N. Clayden, M. Reading, and D. Q. M. Craig, "Characterisation and Prediction of Phase Separation in Hot-Melt Extruded Solid Dispersions: a Thermal, Microscopic and NMR Relaxometry Study," *Pharmaceutical Research* 27, no. 9 (2010): 1869–1883, https://doi.org/10.1007/s11095-010-0185-8.

Supporting Information

Additional supporting information can be found online in the Supporting Information section.

Supporting File: mame70122-sup-0001-SuppMat.docx.